Seasonal and Sub-Seasonal Circulation Anomalies Associated with Persistent Rainy Days in 2018/2019 Winter in Shanghai, China

Wei WANG[1], Fei XIN[2*], Xiao PAN[3], Ying ZHANG[4], and Tim LI[3,5]

1 *Minhang District Office of Shanghai Meteorological Service, China Meteorological Administration, Shanghai* 201199, *China*
2 *Shanghai Climate Center, Shanghai* 200030, *China*
3 *Key Laboratory of Meteorological Disaster, Ministry of Education (KLME)/Joint International Research Laboratory of Climate and Environmental Change (ILCEC)/Collaborative Innovation Center on Forecast and Evaluation of Meteorological Disasters (CIC-FEMD), Nanjing University of Information Science & Technology, Nanjing* 210044, *China*
4 *Ningde Branch of Fujian Meteorological Bureau, China Meteorological Administration, Ningde* 352100, *China*
5 *Department of Atmospheric Sciences, School of Ocean and Earth Science and Technology, University of Hawaii, Honolulu, HI* 96822, *USA*

(Received September 24, 2019; in final form December 5, 2019)

ABSTRACT

Shanghai experienced the longest rainy days in 2018/2019 winter since 1988. The physical cause of such an unusual climate condition was investigated through the diagnosis of observational data. From a seasonal perspective, a long persistent rainy winter was often associated with an El Niño condition in the equatorial Pacific. This abnormal oceanic condition induces a remote teleconnection pattern with pronounced low-level southerly anomalies over East China. The wind anomalies transported moisture from tropical oceans and caused persistent rainfall in East Asia. Meanwhile, the local rainfall time series exhibited a strong quasi-biweekly oscillation (QBWO). Three persistent rainy events were identified in the 2018/2019 winter and they all occurred during the active phase of the QBWO. The first two events were associated with a low pressure anomaly west of Shanghai. Southerly anomalies associated with the low pressure system advected high mean moisture into central eastern China, leading to the persistent rainfall there. The third event was associated with a high pressure anomaly in lower troposphere to the east of Shanghai, which induced anomalous southerlies to its west, favoring the occurrence of rainfall in Shanghai. The result suggests the importance of high-frequency variability in affecting seasonal rainfall anomalies.

Key words: seasonal, sub-seasonal, circulation anomalies, persistent rainy days, El Niño, quasi-biweekly oscillation (QBWO)

Citation: Wang, W., F. Xin, X. Pan, et al., 2020: Seasonal and sub-seasonal circulation anomalies associated with persistent rainy days in 2018/2019 winter in Shanghai, China. *J. Meteor. Res.*, **34**(2), 304–314, doi: 10.1007/s13351-020-9163-1.

1. Introduction

Climatological seasonal wind in central East China in boreal winter is characterized by pronounced northerlies (Li, 2010). Such winds advect dry and cold air southward, leading to a minimum in seasonal rainfall in the region. The 2018/2019 winter, however, experienced an unusual wet season in Shanghai, which was characterized by persistent rain throughout the season. This motivates us to investigate the physical cause of this unusual seasonal climate condition.

One possible cause of the unusual rainy season is attributed to the change of winter mean circulation associated with the El Niño–Southern Oscillation (ENSO). For instance, it is well known that during El Niño mature winter, an anomalous large-scale anticyclone develops over the tropical western North Pacific (Chang et al., 2000a, b; Wang et al., 2000; Li et al., 2017). This anomalous anticyclone is possibly caused by a combined effect of local air–sea interaction mechanism (Wang et al.,

Supported by the National Key Research and Development Program of China (2018YFC1505806), US NOAA (NA18OAR4310298), US NSF (AGS-1643297), National Natural Science Foundation of China (41875069, 41575052, and 41575043), University of Hawaii SOEST (10867), IPRC (1418), and ESMC (294), and National Key Research and Development Program of China Health Risk Assessment Program (2018YFA0606203).

*Corresponding author: xifei010@aliyun.com.

2000) and moist enthalpy advection mechanism (Wu et al., 2017a, b) during its initiation stage [see Li and Hsu (2018) for a thorough review on this subject]. Anomalous southerlies to the west of the anomalous anticyclone transport high mean moisture northward, causing positive rainfall anomalies over South China during El Niño mature winter (Wang et al., 2003; Wu et al., 2010). This remote forcing effect is asymmetric between El Niño and La Niña, due to the intensity and pattern asymmetry between the anomalous anticyclone during El Niño and the anomalous cyclone during La Niña (Wang et al., 2019).

In addition to the seasonal mean circulation change, sub-seasonal modes may also alter large-scale circulation and contribute, to a certain extent, to rainfall activity (Madden and Julian, 1971, 1972; Wang and Rui, 1990; Chatterjee and Goswami, 2004; Jiang et al., 2004; Jiang and Li, 2005; Li and Wang, 2005; Wen et al., 2010; Li, 2014; Xu et al., 2017; Zhu et al., 2017; Qi et al., 2019). It has been shown that there are marked quasi-biweekly and higher-frequency intraseasonal oscillations over East Asia in boreal winter (e.g., Yao et al., 2014; Yang and Li, 2016, 2017). For example, Yao et al. (2014) noted that strong intraseasonal variation of precipitation occurred in South China in boreal winter, and the rainfall variability was associated with the southeastward propagation of the quasi-biweekly mode that originated from the high latitudes. The surface air temperature in mid- and high-latitude Eurasia in boreal winter also exhibited a strong intraseasonal fluctuation (Yang and Li, 2016). Coupled with upper-tropospheric anomalous geopotential height, the signal of near surface temperature propagated southeastward over East Asia. A wave activity flux (WAF) analysis showed that Rossby wave energy dispersion caused the wave train to propagate southeastward. The source of the Rossby wave train appeared over the high-latitude Europe/Atlantic sector, where there was the maximum convergence of WAF. There was barotropic energy conversion from the mean flow to the intraseasonal perturbation during its southeastward journey.

The objective of the current study is to examine the physical cause of persistent rainy season in Shanghai during the 2018/2019 winter from both the seasonal and sub-seasonal circulation change perspective. The remaining part of this paper is organized as follows. In Section 2, the data and method are introduced. In Section 3, we examine seasonal abnormal conditions associated with the persistent rainy day in Shanghai during the past 32 years and compare the conditions with those in the 2018/2019 winter. In Section 4, we further examine sub-seasonal circulation patterns and their evolutions associated with the persistent rainfall in the 2018/2019 winter. Finally, the conclusions and discussion are given in Section 5.

2. Data and analysis method

The primary observational data used in the current study include 1) daily station rainfall data in Xujiahui Station, a station that holds the longest meteorological record in Shanghai, 2) the NCEP/Department of Energy (DOE) Reanalysis II (Kanamitsu et al., 2002), 3) NOAA Climate Prediction Center (CPC) Merged Analysis of Precipitation (CMAP) data, and 4) NOAA Extended Reconstructed Sea Surface Temperature (ERSST) v4 dataset. Both the reanalysis and CMAP products have a horizontal resolution of 2.5° × 2.5°, whereas the ERSST has a horizontal resolution of 2° × 2°. The analysis focuses on boreal winter season (i.e., from December to February) for the period of 1988–2019.

A persistent rainy day index is defined as the number of rainy days within a 3-month period (from 1 December to 28 February) with daily rainfall amount no less than 0.1 mm. According to this definition, 2018/2019 winter became the year of longest rainy days in Shanghai in the past 32 years (Fig. 1). There were a total of 49 rainy days within the three months.

A regression analysis is further employed, to derive the seasonal mean circulation and rainfall anomaly patterns associated with the rainy day index. This analysis will illustrate favorable tropical SST and circulation patterns associated with the persistent rainfall in Shanghai.

A power spectrum analysis is applied to illustrate the

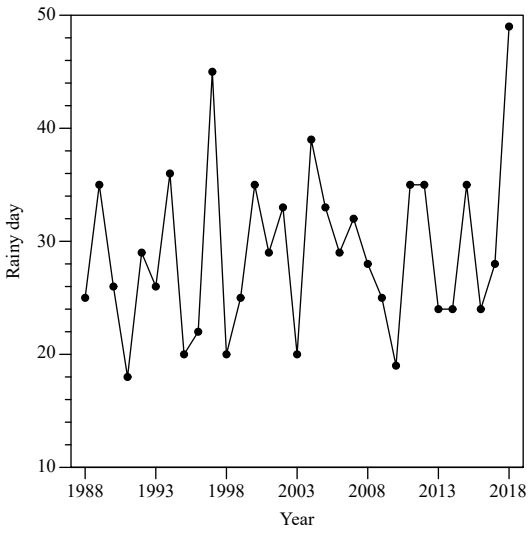

Fig. 1. Time evolution of the persistent rainy day index during the past 32 years.

dominant period of sub-seasonal rainfall variation in Shanghai Station. Once the dominant period is known, a Lanczos bandpass filtering is further applied to all datasets to retain the intraseasonal signals.

To illustrate Rossby wave energy propagation in the upper troposphere, we adopt phase-independent wave activity formula (Takaya and Nakamura, 2001). The Rossby wave activity flux may be written as

$$\boldsymbol{W} = \frac{1}{2|\overline{\boldsymbol{U}}|}\begin{bmatrix} \overline{u}\left(\psi_x'^2 - \psi'\psi'_{xx}\right) + \overline{v}\left(\psi'_x\psi'_y - \psi'\psi'_{xy}\right) \\ \overline{u}\left(\psi'_x\psi'_y - \psi'\psi'_{xy}\right) + \overline{v}\left(\psi_y'^2 - \psi'\psi'_{yy}\right) \end{bmatrix}, \quad (1)$$

where $\overline{\boldsymbol{U}}$, $\overline{u}$, and $\overline{v}$ represent the climatological seasonal mean horizontal, zonal, and meridional winds, ψ' denotes intraseasonal perturbation stream function, and subscripts denote partial derivatives at zonal or meridional directions. The wave activity flux represents Rossby wave energy propagation direction.

3. Seasonal mean circulation patterns associated with the rainy day index

Figure 1 shows that the Shanghai persistent rainy day index exhibits a strong interannual fluctuation. In some years, the number of total rainy day exceeds 35 days, while in other years the number of total rainy day is about 20 days or lower. The maximum rainy day index occurred in 2018/2019 winter, followed by 1997/1998 winter.

To illustrate large-scale atmospheric and oceanic conditions associated with the large rainy day index, we conducted a regression analysis by regressing SST, precipitation, specific humidity, relative humidity, and wind fields onto the index during 1988–2019. Figure 2 shows the regression result. It is interesting to note that an El Niño like SST pattern appears over the tropical Pacific (Fig. 2a). Associated with this SST pattern is pronounced westerly anomaly and enhanced rainfall over the equatorial central Pacific. In the East Asia–western North Pacific sector, there is a low-level anomalous anticyclone (Li et al., 2017). Anomalous northerly to the east of the anticyclone co-locates with cold SST anomaly (SSTA) and negative precipitation anomaly (Figs. 2a, b), confirming the local air–sea interaction mechanism (Wang et al., 2000) and moist enthalpy advection mechanism (Wu et al., 2017a, b). To the west of the anticyclone is pronounced southerly anomaly (Fig. 2a), which advects tropical moist and warm air northward, providing moisture and latent energy source over South and central China (Fig. 2c).

The circulation patterns shown in Fig. 2 were derived

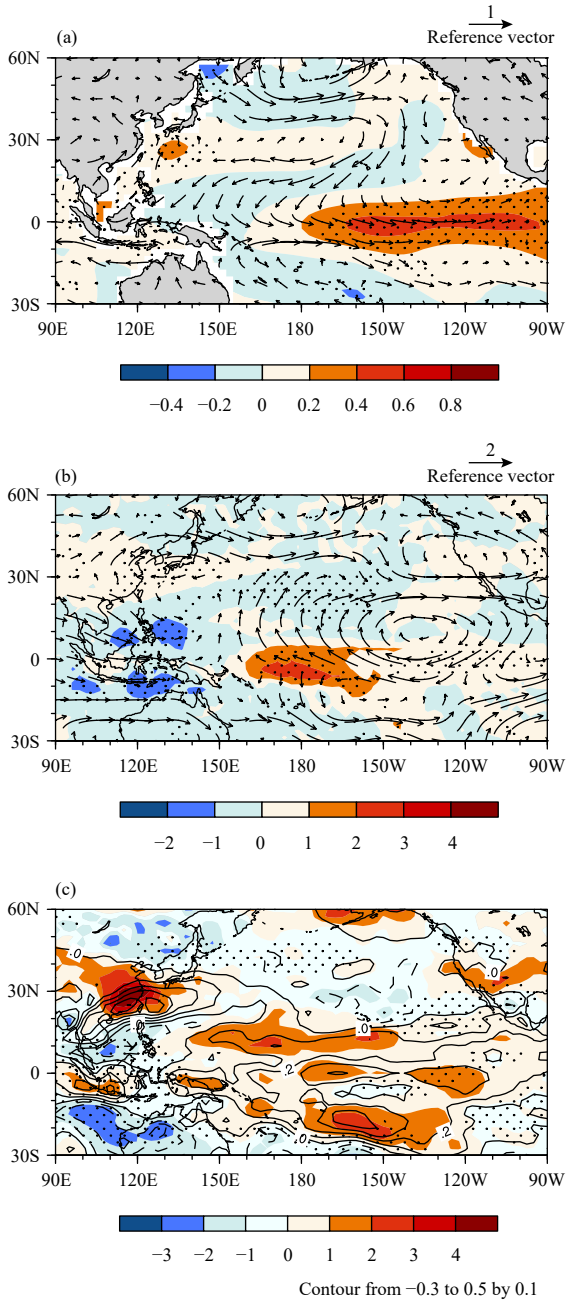

Fig. 2. The horizontal patterns of (a) anomalous SST (shaded; °C; black dots denote 90% confidence level) and 850-hPa wind fields (vector; m s^{-1}), (b) anomalous precipitation (shaded; mm day^{-1}; black dots denote 90% confidence level) and 200-hPa wind fields (vector; m s^{-1}), and (c) anomalous 850-hPa relative humidity (shaded; %) and specific humidity (contour; g kg^{-1}; black dots denote 90% confidence level) fields regressed onto the persistent rainy day index for 1988–2019.

from the regression analysis. They illustrate general large-scale circulation conditions for a long persistent rainy winter in Shanghai during the past 32 years. Next, we compare the circulation feature above to those in 2018/2019 winter. Figure 3 shows the anomalous seasonal

circulation patterns during that particular winter. Note that the SST, wind, moisture, and precipitation patterns are in general similar to those derived from the regression. The most robust common features that appeared in both figures are an El Niño like warming pattern and pronounced southerly anomalies over East China. There are also some notable differences. For instance, equatorial SSTA in 2018/2019 winter was stronger than the regressed SSTA amplitude, and the associated equatorial precipitation anomaly was also stronger and shifted further westward (Figs. 3a, b). The area of enhanced moisture anomalies appeared confined more over central and South China (Fig. 3c).

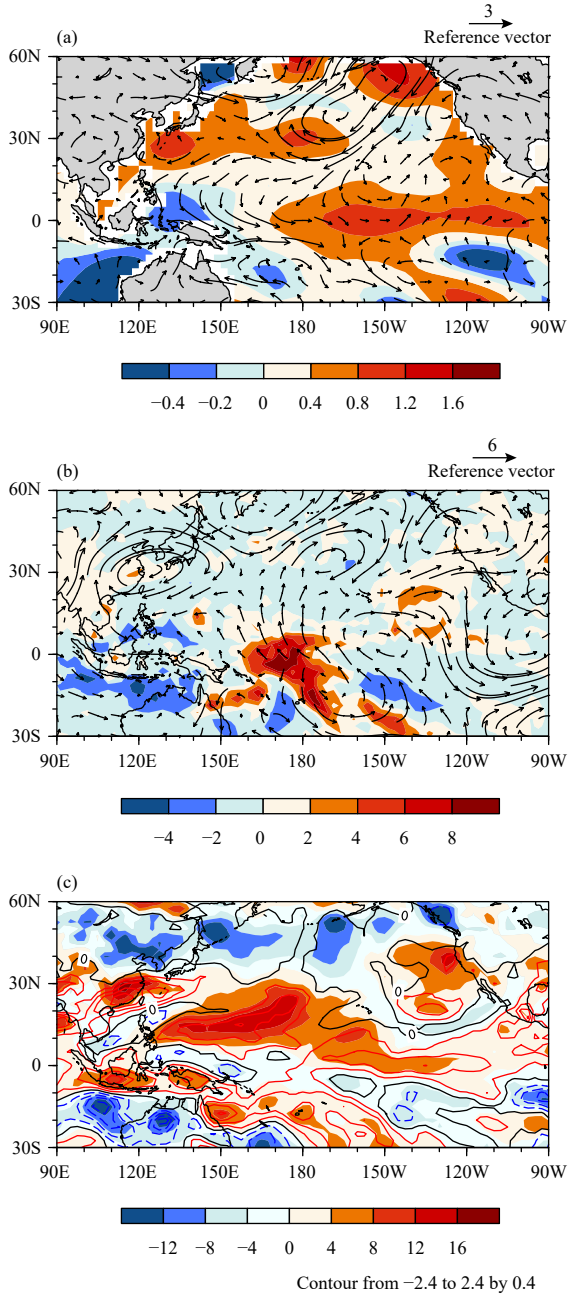

Fig. 3. The horizontal patterns of (a) anomalous SST (shaded; °C) and 850-hPa wind fields (vector; m s^{-1}), (b) anomalous precipitation (shaded; mm day^{-1}) and 200-hPa wind fields (vector; m s^{-1}), and (c) anomalous 850-hPa relative humidity (shaded; %) and specific humidity (contour; g kg^{-1}) fields averaged in 2018/2019 winter season.

The result above describes the favorable conditions of seasonal SST and circulation anomalies for persistent rainfall in Shanghai in 2018/2019 winter. In the next section, we further examine the sub-seasonal circulation patterns and their evolutions in association with the persistent rainfall in Shanghai.

4. Role of sub-seasonal events in affecting the persistent rainfall in Shanghai

A power spectrum analysis was carried out to reveal the dominant period of daily rainfall in Shanghai Station during the 2018/2019 winter. Figure 4a shows the analysis result. A most significant peak appears in 10–25 days, indicating that the sub-seasonal variability is dominated by the quasi-biweekly oscillation (QBWO) during the period.

A persistent rainy event is defined as follows: there are at least 4 rainy days within a 5-day interval or at least 7 rainy days within a 10-day interval. Here, a rainy day is defined when daily amount of rain is no less than 0.1 mm per day. According to this definition, three persistent rainy events were derived during the 2018/2019 winter: Event 1 for 2–11 December, Event 2 for 4–12 January, and Event 3 for 7–22 February.

To illustrate the relationship between the persistent rainy events and the QBWO mode, we plotted the daily rain amount and the quasi-biweekly rain time series together in Fig. 4b. Note that the identified persistent rainy events happened during the active phase of the QBWO mode, implying that the persistent rainy events were closely related to the QBWO.

Figure 5 shows the vertical profiles of vertical velocity and specific humidity anomalies averaged over the three rainy events. Note that there was a marked ascending motion anomaly in Shanghai associated with each of the rainy events. Accompanied with the ascending motion were positive specific humidity anomalies throughout the most of the troposphere. Maximum specific humidity appeared at 700 hPa. In addition, relative humidity anomalies were also positive throughout the troposphere. These large-scale moisture conditions favored the development of persistent rainy events in the region.

To reveal the origin of the large-scale ascending motion and moisture sources, we examine the evolution of the circulation pattern for each event. Figure 6 shows the

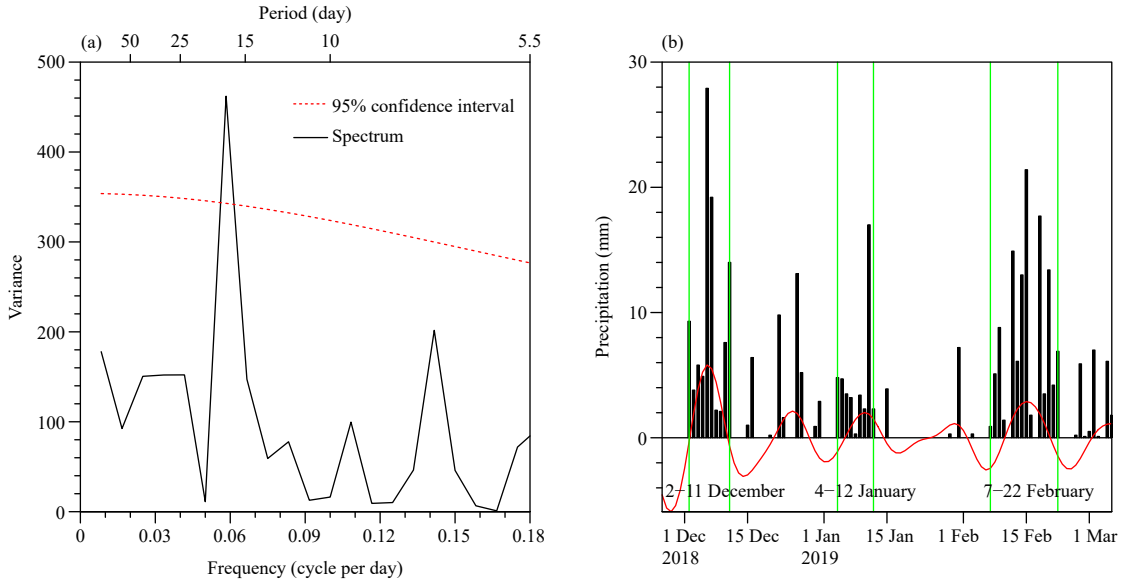

Fig. 4. (a) Power spectrum of daily rain time series during the 2018/2019 winter in Shanghai, with the red dashed curve denoting the 95% confidence level. (b) Daily precipitation amount (bar), the three persistent rainy events (green lines), and the 10–25-day filtered rainfall anomaly (red curve) in Shanghai.

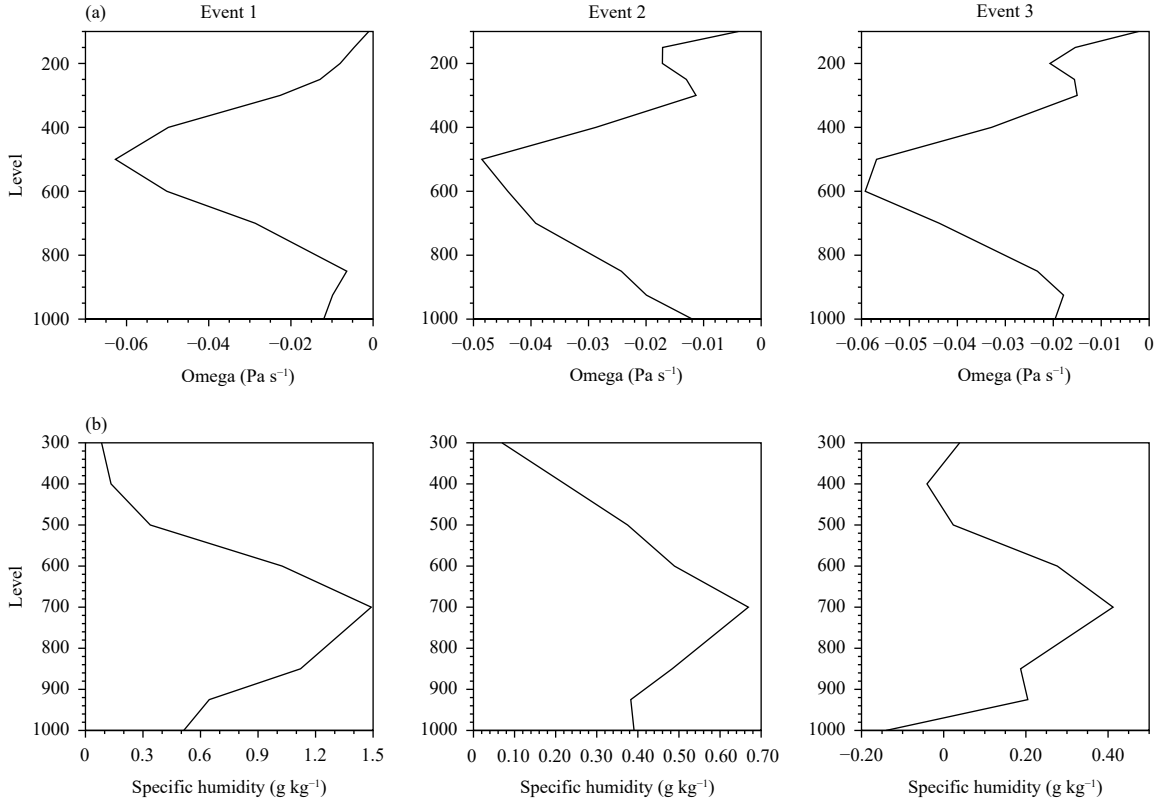

Fig. 5. Vertical profiles of (a) vertical *p*-velocity (omega; Pa s^{-1}) and (b) specific humidity (g kg^{-1}) anomalies associated with the quasi-biweekly mode averaged during the periods of the three persistent rainy events occurring in the 2018/2019 winter.

vertical motion, relative humidity, and geopotential height fields associated with the first event. The ascending motion anomaly appeared originated from northern China, propagating from 40°N on 30 November to about 30°N on 6 December. A similar propagation characteristic was also found in 850-hPa geopotential height field. Pronounced southerly anomalies to the east of the low pressure anomaly center persisted from 30 November to 6

December, leading to northward moisture transport and thus the first persistent rainy event.

Associated with the low-level circulation evolution is the development of a wave train in the upper tropo-

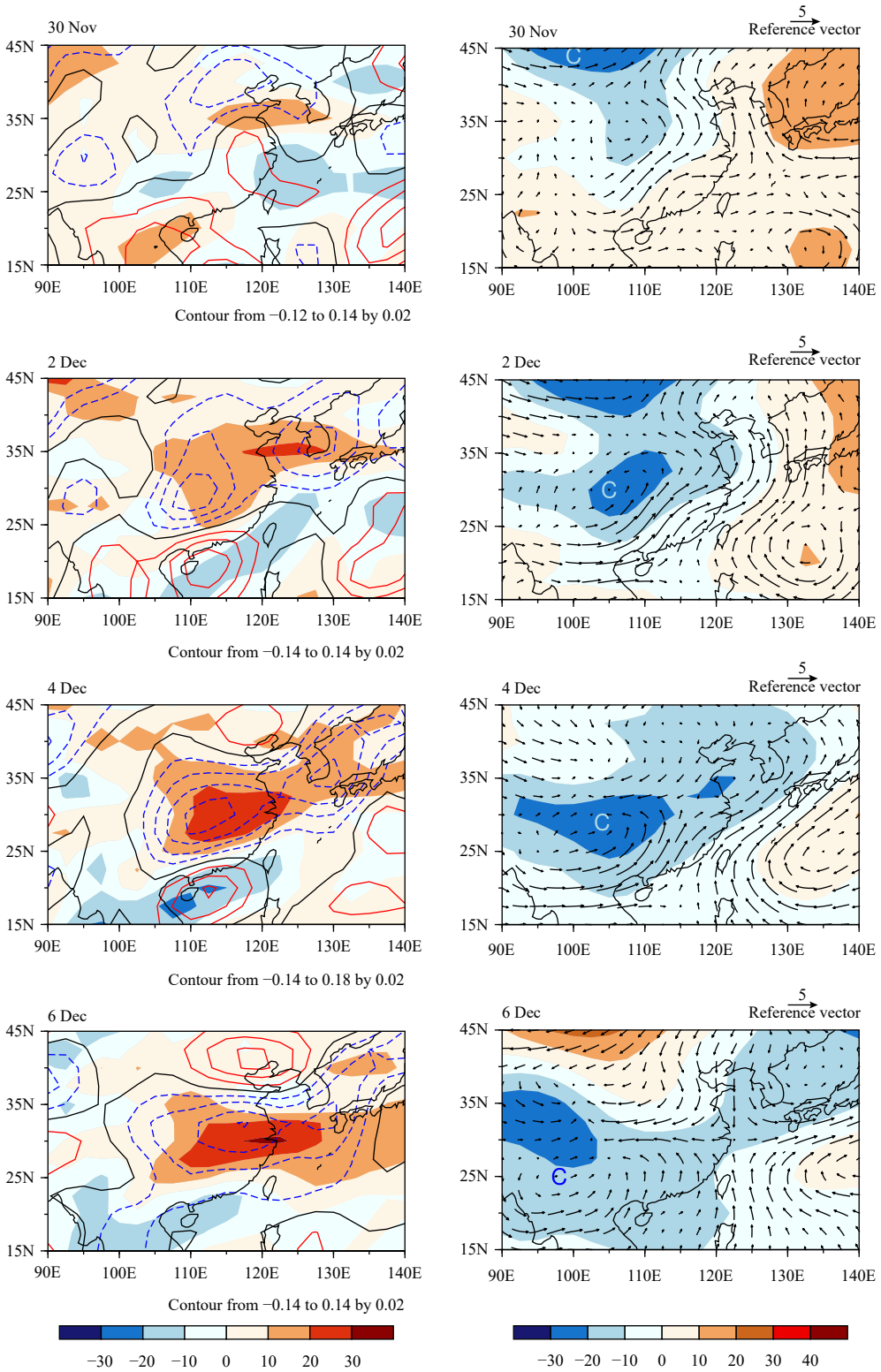

Fig. 6. Evolutions of (left) 700-hPa relative humidity (shaded; %) and 500-hPa vertical *p*-velocity (contour; Pa s^{-1}) anomaly fields and (right) 850-hPa geopotential height (shaded; gpm) and wind (vector; m s^{-1}) anomaly fields associated with the QBWO from 30 November to 6 December 2018. Letter "C" denotes the anomalous cyclonic center that affected rainfall in Shanghai.

sphere (Fig. 7). A positive geopotential height center at 200 hPa appeared around 60°N, 40°E on 30 November, and then moved eastward. Meanwhile, a negative height center appeared at 70°N, 100°E on 30 November, and then moved southeastward. A northwest–southeast oriented wave train was clearly seen on 2 December 2018. The wave train intensified as it propagated eastward.

The formation of the upper-tropospheric wave train was caused by Rossby wave energy dispersion, as seen from the upper-tropospheric wave activity flux field (Fig. 8a). Given the equivalent barotropic vertical structure of the wave train (Fig. 8b), the low-frequency development and evolution of the upper-tropospheric wave train were at least partially responsible for the maintenance of the low pressure system at 850 hPa west of Shanghai.

The second persistent rainy event was also associated with the southward progression of ascending motion anomaly from 40°N on 4 January to near 30°N on 10 January (Fig. 9). The geopotential height anomaly at 850 hPa showed a similar southward migration, even though the low pressure center appeared west of the anomalous ascending motion center. Physically it is reasonable because ascending motion usually appears to the east of a trough, according to the quasi-geostrophic dynamics.

Again, pronounced southerly anomalies to the east of the low-level low pressure system persisted for a few

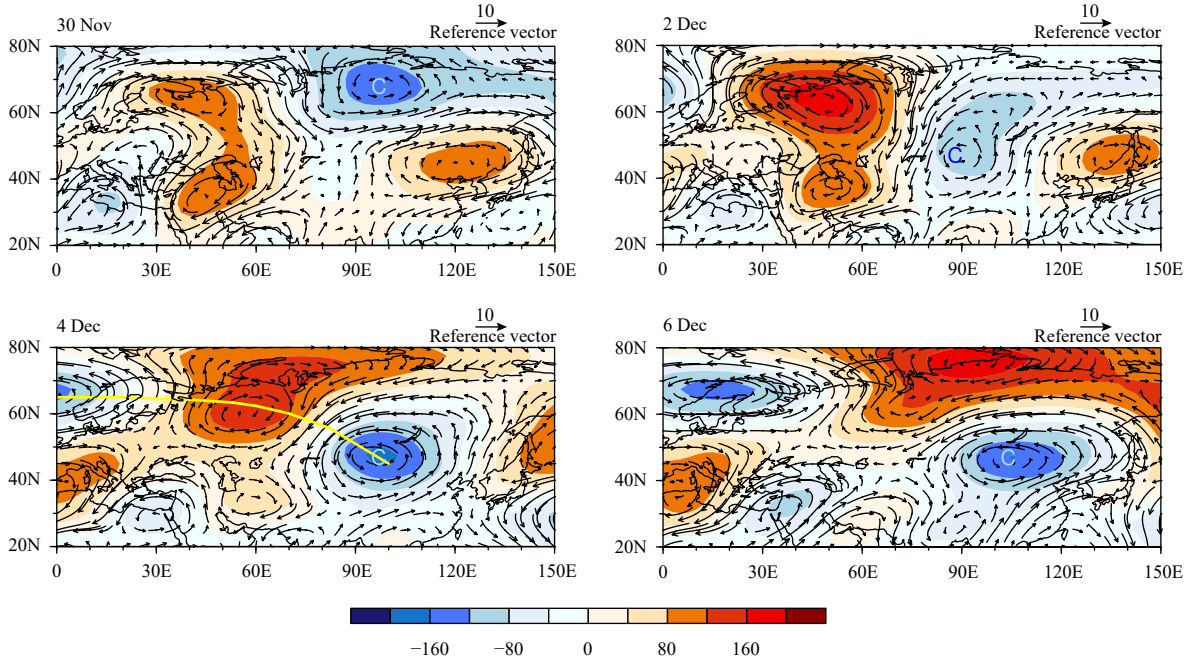

Fig. 7. Evolutions of 200-hPa wind (vector; m s^{-1}) and geopotential height (shaded; gpm) anomaly fields associated with the QBWO from 30 November to 6 December 2018. Yellow curve denotes a wave train that connects anomalous cyclonic and anticyclonic centers.

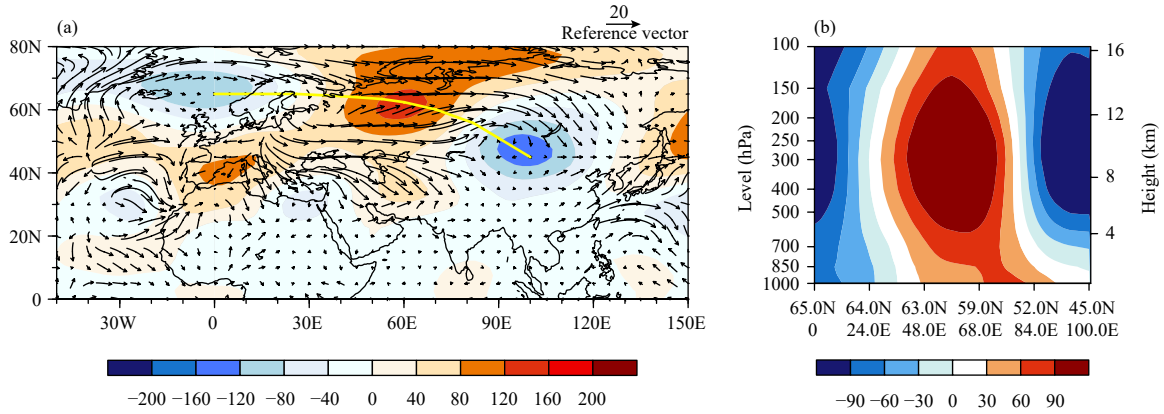

Fig. 8. (a) Horizontal patterns of wave activity flux (vector; m^2 s^{-2}) and geopotential height anomaly (shaded; gpm) fields at 200 hPa and (b) vertical cross-section of the geopotential height anomaly (shaded; gpm) along the wave train direction [i.e., yellow line in (a)], averaged for the period of 2–6 December 2018.

days, from 4 to 10 January 2019 (Fig. 9). These winds were against the winter mean climatological flow, and caused the increase of moisture in Shanghai. Such low-frequency circulation and moisture patterns favored the

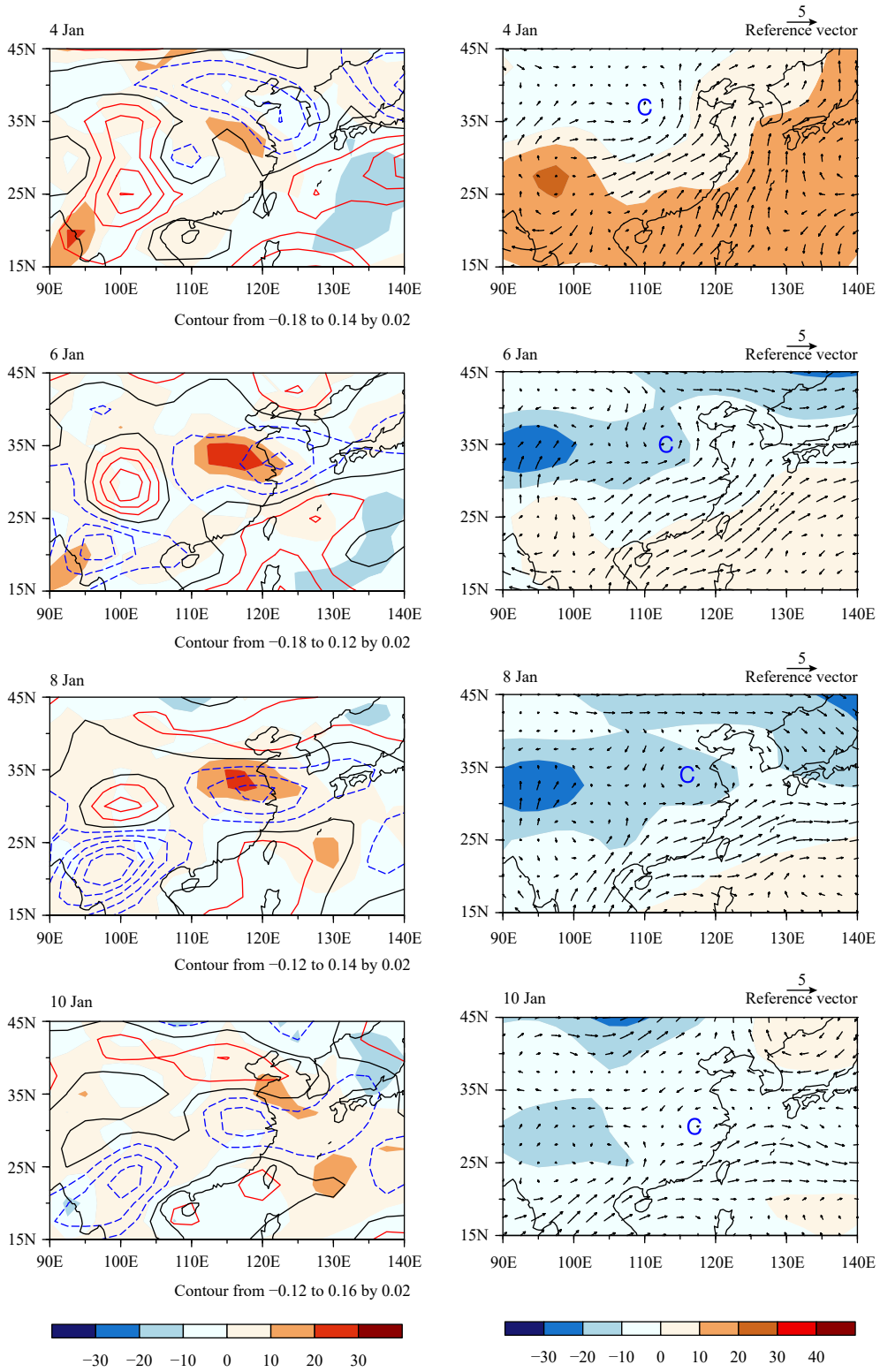

Fig. 9. Evolutions of (left) 850-hPa relative humidity (shaded; %) and 500-hPa vertical *p*-velocity (contour; Pa s^{-1}) and (right) 850-hPa geopotential height (shaded; gpm) and wind (vector; m s^{-1}) anomalies during the second persistent rainy event from 4 to 10 January 2019. Letter "C" denotes the anomalous cyclonic center that affected Shanghai rainfall.

development and maintenance of rainfall in the region.

Different from the first event, the upper-tropospheric wave train pattern was not clearly presented during the second rainy event (figure omitted). This suggests that

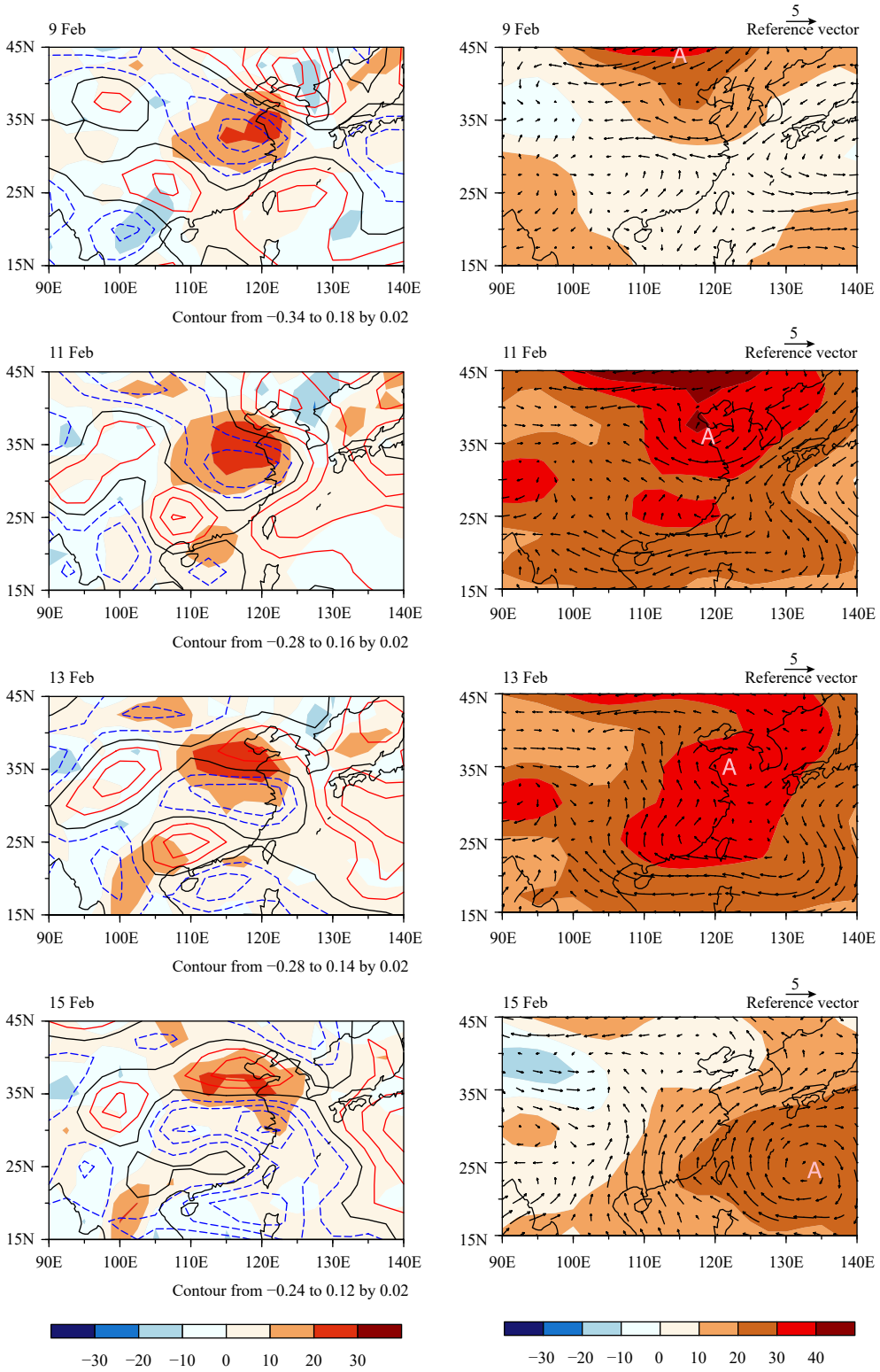

Fig. 10. Evolutions of (left) 925-hPa relative humidity (shaded; %) and 600-hPa vertical *p*-velocity (contour; Pa s^{-1}) and (right) 850-hPa geopotential height (shaded; gpm) and wind (vector; m s^{-1}) anomalies during the third persistent rainy event from 9 to 15 February 2019. Letter "A" denotes the anomalous anticyclonic center.

the second event was primarily caused by low-frequency wind anomalies in lower troposphere.

Anomalous circulation patterns associated with the third rainy event were quite distinctive from the first two events in that a high pressure anomaly, rather than a low pressure anomaly, appeared in lower troposphere (Fig. 10, right panel). The high pressure anomaly was located along the coast of China. It induced a low-level anticyclonic flow, with pronounced southerly anomalies appearing to the west of the high pressure center. Because of the persistence of the high pressure system, the southerly anomalies also persisted. They were responsible for the increase of local moisture in Shanghai (Fig. 10, left panel) and were thus responsible for the occurrence of the third rainy event.

5. Conclusions and discussion

The observational analysis of daily rainfall in Shanghai Station shows that the 2018/2019 winter possessed the longest rainy days since 1988. What caused such a distinctive characteristic was investigated from both the seasonal and sub-seasonal circulation change perspective. A regression analysis using the past 32-yr data indicates that statistically a long persistent rainy winter appeared when an El Niño happened in the equatorial Pacific. The positive SST anomaly in the eastern equatorial Pacific may induce a teleconnection pattern in the East Asian coast and western North Pacific, causing southerly anomalies over East China. The moisture transport associated with the southerly anomalies favored the occurrence and maintenance of rainfall over Shanghai region. The SST, circulation, and moisture patterns in 2018/2019 winter in general resembled those derived from the regression analysis.

A further analysis of power spectrum of daily rainfall in Shanghai Station reveals that the rainfall time series was dominated by a 10–25-day period, and each of the persistent rainy events was associated with the QBWO mode. In total, three persistent rainy events were identified for the 2018/2019 winter. The first two events were associated with a low pressure anomaly system in the upstream, which gradually propagated southeastward. Low-level southerly anomalies associated with the low pressure system advected abundant moisture from tropical oceans to central China, leading to the persistent rainfall events. The third event, on the other hand, was associated with a high pressure anomaly system over and to the east of Shanghai region. Anomalous southerlies to the west of the positive pressure anomaly favored low-level moisture transport and thus the occurrence of rainfall.

The observational analysis above suggests that the exceptional longest rainy days in 2018/2019 winter were attributed to both the favorable seasonal mean flow and the strong sub-seasonal variability. Therefore, there is urgent need to conduct sub-seasonal to seasonal predictions in order to forecast exceptional climate events such as that over Shanghai in 2018/2019 winter.

While the current analysis points out the importance of upscale feedback of the sub-seasonal mode on seasonal mean climate anomalies, it is not clear how the sub-seasonal mode variability was influenced by the seasonal circulation anomaly and what specific processes through which the sub-seasonal mode could feed back to the interannual anomaly were. For example, in the feedback of higher-frequency modes to lower-frequency variability, does a higher intensity of the QBWO correspond to a greater seasonal mean precipitation anomaly (Qi et al., 2008; Li et al., 2015)? If this is the case, then a simple linear accumulation would work. On the other hand, it would be interesting to understand the nonlinear rectification process (Zhou and Li, 2010; Hsu and Li, 2011; Hsu et al., 2011). For example, a positive (negative) boundary layer convergence anomaly and a positive (negative) moisture anomaly in situ associated with the QBWO mode would lead to a strengthening (weakening) of seasonal mean precipitation through an upscale feedback process similar to that proposed by Zhu et al. (2019). If both the linear and nonlinear processes were operated, one may further address their relative importance. These issues require further in-depth diagnoses and theoretical and modeling investigations.

REFERENCES

Chang, C.-P., Y. S. Zhang, and T. Li, 2000a: Interannual and interdecadal variations of the East Asian summer monsoon and tropical Pacific SSTs. Part I: Roles of the subtropical ridge. *J. Climate*, **13**, 4310–4325, doi: 10.1175/1520-0442(2000)013<4310:IAIVOT>2.0.CO;2.

Chang, C.-P., Y. S. Zhang, and T. Li, 2000b: Interannual and interdecadal variations of the East Asian summer monsoon and tropical Pacific SSTs. Part II: Meridional structure of the monsoon. *J. Climate*, **13**, 4326–4340, doi: 10.1175/1520-0442(2000)013<4326:IAIVOT>2.0.CO;2.

Chatterjee, P., and B. N. Goswami, 2004: Structure, genesis and scale selection of the tropical quasi-biweekly mode. *Quart. J. Roy. Meteor. Soc.*, **130**, 1171–1194, doi: 10.1256/qj.03.133.

Hsu, P.-C., and T. Li, 2011: Interactions between boreal summer intraseasonal oscillations and synoptic-scale disturbances over the western North Pacific. Part II: Apparent heat and moisture sources and eddy momentum transport. *J. Climate*, **24**, 942–961, doi: 10.1175/2010JCLI3834.1.

Hsu, P.-C., T. Li, and C.-H. Tsou, 2011: Interactions between boreal summer intraseasonal oscillations and synoptic-scale disturbances over the western North Pacific. Part I: Energet-

ics diagnosis. *J. Climate*, **24**, 927–941, doi: 10.1175/2010JCLI3833.1.

Jiang, X. A., and T. Li, 2005: Reinitiation of the boreal summer intraseasonal oscillation in the tropical Indian Ocean. *J. Climate*, **18**, 3777–3795, doi: 10.1175/JCLI3516.1.

Jiang, X. A., T. Li, and B. Wang, 2004: Structures and mechanisms of the northward propagating boreal summer intraseasonal oscillation. *J. Climate*, **17**, 1022–1039, doi: 10.1175/1520-0442(2004)017<1022:SAMOTN>2.0.CO;2.

Kanamitsu, M., W. Ebisuzaki, J. Woollen, et al., 2002: NCEP–DOE AMIP-II Reanalysis (R-2). *Bull. Amer. Meteor. Soc.*, **83**, 1631–1644, doi: 10.1175/BAMS-83-11-1631.

Li, C. H., T. Li, A. L. Lin, et al., 2015: Relationship between summer rainfall anomalies and sub-seasonal oscillations in South China. *Climate Dyn.*, **44**, 423–439, doi: 10.1007/s00382-014-2172-y.

Li, T., 2010: Monsoon climate variabilities. *Climate Dynamics*: *Why Does Climate Vary*? Sun, D.-Z., and F. Bryan, Eds., American Geophysical Union, Washington, 27–51, doi: 10.1029/2008GM000782.

Li, T., 2014: Recent advance in understanding the dynamics of the Madden–Julian oscillation. *J. Meteor. Res.*, **28**, 1–33, doi: 10.1007/s13351-014-3087-6.

Li, T., and B. Wang, 2005: A review on the western North Pacific monsoon: Synoptic-to-interannual variabilities. *Terr. Atmos. Oceanic Sci.*, **16**, 285–314, doi: 10.3319/TAO.2005.16.2.285(A).

Li, T., and P.-C. Hsu, 2018: *Fundamentals of Tropical Climate Dynamics*. Springer, Cham, 229 pp, doi: 10.1007/978-3-319-59597-9.

Li, T., B. Wang, B. Wu, et al., 2017: Theories on formation of an anomalous anticyclone in western North Pacific during El Niño: A review. *J. Meteor. Res.*, **31**, 987–1006, doi: 10.1007/s13351-017-7147-6.

Madden, R. A., and P. R. Julian, 1971: Detection of a 40–50 day oscillation in the zonal wind in the tropical Pacific. *J. Atmos. Sci.*, **28**, 702–708, doi: 10.1175/1520-0469(1971)028<0702:DOADOI>2.0.CO;2.

Madden, R. A., and P. R. Julian, 1972: Description of global-scale circulation cells in the tropics with a 40–50 day period. *J. Atmos. Sci.*, **29**, 1109–1123, doi: 10.1175/1520-0469(1972)029<1109:DOGSCC>2.0.CO;2.

Qi, Y. J., R. H. Zhang, T. Li, et al., 2008: Interactions between the summer mean monsoon and the intraseasonal oscillation in the Indian monsoon region. *Geophys. Res. Lett.*, **35**, L17704, doi: 10.1029/2008GL034517.

Qi, Y. J., T. Li, R. H. Zhang, et al., 2019: Interannual relationship between intensity of rainfall intraseasonal oscillation and summer-mean rainfall over Yangtze River Basin in eastern China. *Climate Dyn.*, **53**, 3089–3108, doi: 10.1007/s00382-019-04680-w.

Takaya, K., and H. Nakamura, 2001: A formulation of a phase-independent wave-activity flux for stationary and migratory quasigeostrophic eddies on a zonally varying basic flow. *J. Atmos. Sci.*, **58**, 608–627, doi: 10.1175/1520-0469(2001)058<0608:AFOAPI>2.0.CO;2.

Wang, B., and H. Rui, 1990: Synoptic climatology of transient tropical intraseasonal convection anomalies: 1975–1985. *Meteor. Atmos. Phys.*, **44**, 43–61, doi: 10.1007/BF01026810.

Wang, B., R. G. Wu, and X. H. Fu, 2000: Pacific–East Asian teleconnection: How does ENSO affect East Asian climate? *J. Climate*, **13**, 1517–1536, doi: 10.1175/1520-0442(2000)013<1517:PEATHD>2.0.CO;2.

Wang, B., R. G. Wu, and T. Li, 2003: Atmosphere–warm ocean interaction and its impacts on Asian–Australian monsoon variation. *J. Climate*, **16**, 1195–1211, doi: 10.1175/1520-0442(2003)16<1195:AOIAII>2.0.CO;2.

Wang, X. H., T. Li, and M. C. Chen, 2019: Mechanism for asymmetric atmospheric responses in the western North Pacific to El Niño and La Niña. *Climate Dyn.*, **53**, 3957–3969, doi: 10.1007/s00382-019-04767-4.

Wen, M., T. Li, R. H. Zhang, et al., 2010: Structure and origin of the quasi-biweekly oscillation over the tropical Indian Ocean in boreal spring. *J. Atmos. Sci.*, **67**, 1965–1982, doi: 10.1175/2009JAS3105.1.

Wu, B., T. Li, and T. J. Zhou, 2010: Asymmetry of atmospheric circulation anomalies over the western North Pacific between El Niño and La Niña. *J. Climate*, **23**, 4807–4822, doi: 10.1175/2010JCLI3222.1.

Wu, B., T. J. Zhou, and T. Li, 2017a: Atmospheric dynamic and thermodynamic processes driving the western North Pacific anomalous anticyclone during El Niño. Part I: Maintenance mechanisms. *J. Climate*, **30**, 9621–9635, doi: 10.1175/JCLI-D-16-0489.1.

Wu, B., T. J. Zhou, and T. Li, 2017b: Atmospheric dynamic and thermodynamic processes driving the western North Pacific anomalous anticyclone during El Niño. Part II: Formation processes. *J. Climate*, **30**, 9637–9650, doi: 10.1175/JCLI-D-16-0495.1.

Xu, Z. Q., T. Li, and K. Fan, 2017: The weakened intensity of the atmospheric quasi-biweekly oscillation over the western North Pacific during late summer around the late 1990s. *J. Climate*, **30**, 9807–9826, doi: 10.1175/JCLI-D-16-0759.1.

Yang, S. Y., and T. Li, 2016: Intraseasonal variability of air temperature over the mid–high latitude Eurasia in boreal winter. *Climate Dyn.*, **47**, 2155–2175, doi: 10.1007/s00382-015-2956-8.

Yang, S. Y., and T. Li, 2017: The role of intraseasonal variability at mid-high latitudes in regulating Pacific blockings during boreal winter. *Int. J. Climatol.*, **37**, 1248–1256, doi: 10.1002/joc.5080.

Yao, S. X., Q. Huang, T. Li, et al., 2014: The intraseasonal oscillations of precipitation and circulations from January to March in 2010 in East Asia. *Meteor. Atmos. Phys.*, **123**, 67–79, doi: 10.1007/s00703-013-0287-z.

Zhou, C. H., and T. Li, 2010: Upscale feedback of tropical synoptic variability to intraseasonal oscillations through the nonlinear rectification of the surface latent heat flux. *J. Climate*, **23**, 5738–5754, doi: 10.1175/2010JCLI3468.1.

Zhu, Y., T. Li, M. Zhao, et al., 2019: Interaction between the MJO and high-frequency waves over the Maritime Continent in boreal winter. *J. Climate*, **32**, 3819–3835, doi: 10.1175/JCLI-D-18-0511.1.

Zhu, Z. W., S. J. Chen, K. Yuan, et al., 2017: Empirical subseasonal prediction of summer rainfall anomalies over the middle and lower reaches of the Yangtze River basin based on atmospheric intraseasonal oscillation. *Atmosphere*, **8**, 185, doi: 10.3390/atmos8100185.

Tech & Copy Editor: Qi WANG